HHS Public Access

Author manuscript

J Phys Chem B. Author manuscript; available in PMC 2021 October 01.

Published in final edited form as:

J Phys Chem B. 2020 October 01; 124(39): 8665–8677. doi:10.1021/acs.jpcb.0c07177.

Temperature-Jump 2D IR Spectroscopy with Intensity-Modulated CW Optical Heating

Brennan Ashwood, **Nicholas H. C. Lewis**, **Paul J. Sanstead**, **Andrei Tokmakoff***

Department of Chemistry, James Franck Institute, and Institute for Biophysical Dynamics, The University of Chicago, Chicago, IL 60637, USA.

Abstract

Pulsed temperature-jump (T-jump) spectroscopy with infrared (IR) detection has been widely used to study biophysical processes occurring from nanoseconds to ~1 millisecond with structural sensitivity. However, many systems exhibit structural dynamics on timescales longer than the millisecond barrier that is set by the time-scale for thermal relaxation of the sample. We have developed a linear and nonlinear infrared spectrometer coupled to an intensity-modulated continuous wave (CW) laser to probe T-jump initiated chemical reactions from <1 ms to seconds. Time-dependent modulation of the CW laser leads to a <1 ms heating time as well as a constant final temperature (± 3%) for the duration of the heating time. Temperature changes of up to 75 °C in D_2O are demonstrated, allowing for nonequilibrium measurements inaccessible to standard pulsed optical T-jump setups. T-jump linear absorption, pump-probe, and two-dimensional IR (2D IR) spectroscopy are applied to the unfolding and refolding of ubiquitin and a model intercalated motif (i-motif) DNA sequence, and analysis of the observed signals is used to demonstrate the limits and utility of each method. Overall, the ability to probe temperature-induced chemical processes from <1 ms to many seconds with 2D IR spectroscopy provides multiple new avenues for time-dependent spectroscopy in chemistry and biophysics.

Graphical Abstract

***Corresponding Author**: tokmakoff@uchicago.edu.

Supporting Information

Sample preparation; Methodology of determining sample temperature change; Details of solvent heating and cooling simulations; T_J-dependent solvent heating and cooling measurements; Methodology of D_2O background removal for t-A spectroscopy; Comparison of t-A and t-PP signal amplitude and relaxation kinetics; Evaluation of distortions in T-jump and T-drop data from overlap with solvent heating and cooling profile, respectively.

The authors declare no competing financial interest.

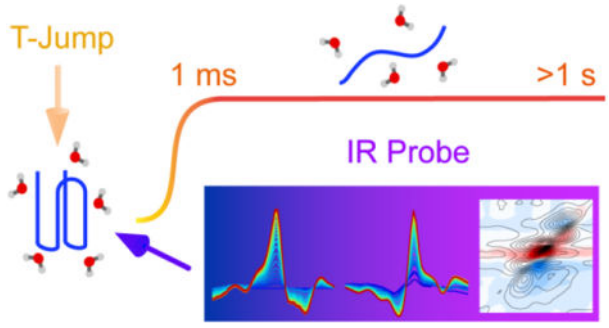

1. Introduction

Macromolecules exhibit structural dynamics spanning from solvation dynamics on picosecond timescales to large secondary structure rearrangements that last from milliseconds to seconds. For the last 50 years, temperature-jump (T-jump) spectroscopy has been one of the most common methods for investigating macromolecule and chemical reaction dynamics due to its ability to probe over many decades in time.[1–5] To generate temperature changes rapid enough to resolve fast molecular motions, T-jumps are typically delivered through electrical discharge[6] or optical excitation of the solvent.[7–11] In the most common optical approach, an intense near-infrared laser with ~10 ns pulses is used to excite the overtone of the O-H or O-D stretching vibration, leading to solvent heating within the envelope of the pulse (< 10 ns). This type of T-jump setup has been instrumental for the investigation of intermediate species and activated and downhill kinetics in processes such as protein unfolding,[12–13] DNA dehybridization,[4, 14] nucleic acid unfolding,[15–16] and various chemical reactions.[17–20] The elevated temperature lasts from ~10 ns to ~1 ms until the sample begins to relax toward the initial temperature (T_i). However, many macromolecules exhibit large changes in secondary structure that are known or proposed to occur from tens to hundreds of milliseconds.[21–27] The millisecond limit to pulsed T-jump experiments is governed by the time scale for thermal diffusion of the initially deposited heat out of the sample, so to access longer time scales, steady-state heating at a rate equal to the rate of dissipation by thermal diffusion is required to maintain a constant elevated temperature. Continuous wave (CW) optical heating has recently been applied to investigate biomolecular dynamics,[28–30] and may be used to extend the time window for T-jump measurements out to hundreds of milliseconds or seconds. To increase the rate of solvent heating and cooling and to achieve larger temperature changes, optical CW T-jump methods are often performed on small sample volumes and probed with fluorescence microscopy.[28, 30] Additionally, T-jump methods utilizing other types of heating methods have been used to study millisecond reaction dynamics.[23–25]

Infrared (IR) spectroscopy is a structurally sensitive probe that has been employed to track T-jump responses from proteins, nucleic acids, and small molecules.[2, 14, 19, 31–37] In DNA or RNA, each nucleobase exhibits a distinct mid-IR spectrum reporting on in-plane vibrational stretching motions that is reshaped upon changes in hydrogen bonding and base stacking.[38–42] The amide I vibrations of proteins are sensitive to hydrogen bonding, allowing them to report on the disruption of secondary structures such as β-sheets and α-helices.[43–44] IR

spectroscopy can resolve individual residues among a large protein or nucleic acid through isotope labelling of certain atoms, and this approach has been coupled with T-jump spectroscopy to resolve detailed mechanisms of protein unfolding.[33, 45–48] Relative to linear IR spectroscopy, two-dimensional IR (2D IR) spectroscopy offers greater insight into the structure of biomolecules and their interactions with the environment. The 2D IR spectrum reports on coupling between vibrational modes, reveals contributions to the linewidth of an IR transition, and can distinguish whether peaks arise from distinct chemical species.[19, 49–50] Changes in line shape and cross-peaks between vibrational modes of DNA bases have been used to report on base pair formation and base stacking as well as the loss of β-sheet character in proteins while the 2D IR line shape provides information on the distribution of environments the molecule experiences.[40–41, 43, 51] Due to the added technical difficulties relative to T-jump linear IR spectroscopy, the development of T-jump 2D IR (t-2D IR) spectrometers has been limited.[7]

Since pulsed T-jump experiments are limited to time scales shorter than 1–10 ms, T-jump experiments with CW laser heating can be used to access longer time delays. To achieve temperature changes >10 °C with CW heating, a high (~10^4 W/cm^2) near-IR excitation power density is needed at the sample. Focusing of a 135 mW near-IR CW source to small volumes (~10 pL) has been shown to generate temperature changes of up to 80 °C in water within a few milliseconds.[28] Such small heating volumes work when combined with techniques such as fluorescence microscopy but are incompatible with linear IR and 2D IR spectroscopic probes due to the ~10× increase in diffraction-limited spot size in going from the visible to mid-IR. Typical 2D IR setups have a mid-IR probe volume between 50 pL and 1 nL, which requires a T-jump excitation volume between 1 and 50 nL to ensure temperature uniformity of the probe region with a Gaussian mode. Therefore, T-jump IR and 2D IR spectroscopy requires a high CW excitation power to achieve sizeable temperature changes. Even with a higher CW excitation power, the greater heating volume needed for IR spectroscopy will also require more time to heat to a stabilized final temperature, since the millisecond time-scale for thermal diffusion limits the time it takes to reach the point of steady-state heating. In addition, CW heating methods have been shown to create unstable final temperatures that may create thermal artifacts in the T-jump response of the sample.[30] One way to accelerate the heating time and remove time-dependent variation in temperature is to rapidly modulate the T-jump laser intensity throughout the heating event. For example, if the T-jump laser initially excites the solvent with a high power for a short amount of time and then drops down to a plateau power, heating to the temperature of the plateau power will occur faster than if a simple square waveform between an off state and the plateau power were used.

In this article we report the design and characterization of a t-2D IR spectrometer for probing chemical processes from <1 ms to seconds. T-jumps are delivered by optical excitation of the solvent with an intense CW laser modulated by an acousto-optic modulator (AOM). The T-jump laser is coupled into a 2D IR spectrometer that has a pump-probe pulse geometry. T-jump experiments can be performed with and without timing synchronization between the T-jump laser and femtosecond mid-IR probe. Temperature changes (ΔT) of up to ~75 °C in D_2O are demonstrated. T-jump linear IR absorption (t-A), pump-probe (t-PP), and t-2D IR spectroscopy are applied to study unfolding and refolding of intercalated motif

(i-motif) DNA and the protein ubiquitin. The T-jump responses are combined with kinetic simulations (see Supporting Information) to characterize potential distortions to the observed signals and establish methods for analyzing T-jump data.

2. Experimental Section

Our T-jump spectrometer is specifically designed to optically heat the sample through weak absorption by the D_2O stretch overtone near 2 μm to ensure uniform heating across the path length of the sample. We use a 30 W Thulium (Tm) CW fiber laser to induce temperature changes of many tens of degrees, and the laser intensity is abruptly modulated by an AOM to optimize the heating time (<1 ms) of the solvent and rapidly turn off the laser. The temperature of the sample is monitored by the change in mid-IR transmission of D_2O. A train of mid-IR pulses probe the sample continuously with a repetition rate of 1 kHz and are detected pulse-by-pulse in a frequency resolved manner with an array. The mid-IR pulses may be split into a series of pulses and delayed relative to one another with high precision motorized stages to measure nonlinear IR signals from the signal. In total, t-A, t-PP, and t-2D IR probes can be used to track the sample after a T-jump. The details of the mid-IR spectrometer and optical heating method are described in the following sections.

2.1 2D IR Spectrometer

Fig. 1 outlines the optical components used to generate, delay, and detect a series of mid-IR pulses for 2D IR spectroscopy. The output of a Ti:sapphire regenerative amplifier (Libra, Coherent) pumps an optical parametric amplifier (OPA, TOPAS C, Light Conversion). The resulting signal and idler undergo collinear difference-frequency generation (DFG) in an $AgGaS_2$ crystal to generate 10 μJ mid-IR pulses with a 90 fs pulse duration. A CaF_2 wedge (0.5 deg, Q131115LJ2, Altechna) reflects about 5% of the mid-IR light to be used as the probe pulse (k_3). The transmitted portion enters a Mach-Zehnder interferometer that uses a pair of 50:50 CaF_2 beamsplitters (Edmund Optics) to split the beam into two arms (k_1 and k_2), create a time delay between the arms (τ_1), and recombine the beams. The output from the Mach-Zehnder interferometer is split into in-phase and π-shifted outputs. The π-shifted portion is focused onto a room-temperature HgCdTe (MCT) detector (MCT5–020-H, Electro-Optical Systems) that measures the interferogram between k_1 and k_2 to be used as a reference to correct for errors τ_1. The in-phase portion is used as the pump for pump-probe measurements and the first two signal generating pulses in 2D IR measurements. Two mirrors mounted on motorized stages (ANT95L, Aerotech) are placed in the k_1 beam path to control τ_1 and the k_3 beam path to control τ_2, the time delay between k_2 and k_3. The stationary k_2 beam is chopped at 500 Hz (Ch, 3501, Newport) and differential detection between unchopped and chopped shots is used to isolate the PP or 2D IR signal from the large transmitted k_3 background. After the interferometer, the polarization of k_1 and k_2 are controlled by sending each through a MgF_2 half waveplate (MWPMFA2–22-WL-UN, Karl Lambrecht Corp.) and ZnSe polarizer (57503, Specac) in motorized rotation mounts (PRM1Z8, Thorlabs). The k_3 beam transmits through a CaF_2 window (WG51050, Thorlabs) to compensate for dispersion and is then fixed to horizontal polarization with a ZnSe polarizer.

The k_1/k_2 (pump) and k_3 (probe) beams are horizontally offset by 1” and each focused by a gold 90° off-axis parabolic mirror (MPD229H-M03, Thorlabs, 2” reflected focal length) into the sample. A diameter of approximately 40 μm ($1/e^2$ in intensity) was measured for each beam by monitoring the transmitted power as a razor blade was scanned across the focus. A temporal duration FWHM of 90 fs was measured for both the pump and probe pulses by interferometric autocorrelation and cross-correlation measurements, respectively, in $AgGaS_2$. The sample is held between two 1 mm thick CaF_2 windows separated by a 50 μm Teflon spacer. The windows are held in a home-built brass jacket that is temperature controlled using a recirculating chiller (Ministat 125, Huber). For chiller setpoints from 0 to 105 °C, the temperature at the sample was measured with a thermocouple in thermal contact to one CaF_2 window and used to calibrate the reported temperatures in this work. In the pump-probe geometry, the pump-induced intensity change on the probe is measured. Therefore, the pump beam is blocked after the sample and the probe beam is focused into a monochromator (Triax 190, Horiba) that disperses the light onto the lower stripe of a 2 × 64 pixel MCT array connected to a boxcar integrator (IR-0144, Infrared Systems Development). The array signal is sampled every millisecond and converted to a digital signal (ADC) before being stored in FIFO memory and readout to the host computer (PC). A ZnSe analyzer set parallel to the polarization of the probe is placed just before the monochromator.

2.2 Optical Heating of Sample

T-jumps are induced by optical excitation of the overtone transition of the O-D stretch vibration in D_2O. A CW Tm fiber laser (TLR-30, IPG Photonics) outputs 30 W of 1.94 μm light. D_2O has a weak absorption coefficient at this wavelength (15 cm^{-1}), which assures that heating is uniform through the 50 μm thick sample. The output is collimated to a beam diameter of 1.5 mm using a Galilean telescope and sent through an AR-coated TeO_2 AOM (M1099-T40L-2(M), Isomet) with a 2 mm active aperture height. A radiofrequency (RF) driver (531C-7, Isomet) converts a sine wave input with programmable amplitude (0 – 1 V) from an arbitrary function generator (AFG) (31101, Tektronix) to a 40 MHz signal of up to 9.7 W, which is used to drive the AOM. The AOM is placed on a manual rotation stage (RP03, Thorlabs) and rotated to the Bragg angle (9.05 mrad). The rise time of the AOM is ~300 ns. A first-order diffraction efficiency of 70–75% is achieved with maximum RF power. The 0^{th} and 1^{st}-order diffracted beams are separated by an angle of 18.10 mrad. After the beams sufficiently separate, the 0^{th} order beam is blocked, and the 1^{st}-order beam is used for optical heating of the sample. To spatially overlap the T-jump beam and the mid-IR pulses, the T-jump beam is focused through a tapered hole in the center of the 1^{st} off-axis parabolic mirror to a diameter of 230 μm ($1/e^2$ in intensity) at the sample. The T-jump beam is focused to a diameter >5× larger than that of the mid-IR beams to ensure uniform heating of the mid-IR probe volume in the dimensions parallel to the windows. After passing through the sample, the T-jump beam exits through a tapered hole in the second parabolic mirror and is blocked.

2.3 Timing Between T-Jump and Mid-IR Probe

The diffraction of the T-jump laser toward the sample is repeatedly turned on and off, creating an alternating cycle in the sample between a high temperature T_f for a timescale τ_{on}

and low temperature T_i for a time τ_{off}, with a total cycling period τ_T that spans from hundreds of milliseconds to seconds in practice (Fig. 2). Mid-IR probe shots arrive at the sample every 1 ms, and are sorted based on their time of arrival after the T-jump laser turns on (τ_{TJ}) and off ($\tau_{TD} = \tau_{TJ} - \tau_{on}$). Hundreds to thousands of measurements as a function of T-jump delay τ_{TJ} and T-drop delay τ_{TD} are acquired per T-jump cycle and are binned logarithmically. The first probe shot arrives between 0 and 1 ms (τ_{TJ}^{1}) after the T-jump laser turns on. τ_{TJ}^{1} can be electronically controlled (synchronous) or allowed to wander (asynchronous) due to the timing mismatch between the T-jump cycle and the 1 kHz repetition rate of the mid-IR probe. When τ_{TJ}^{1} is allowed to wander, different τ_{TJ}^{1} values are probed in subsequent T-jump cycles. Therefore, asynchronous acquisition is advantageous for collecting data at many time delays, because data at every τ_{TJ} and τ_{TD} will be accumulated together over many T-jump cycles. Synchronous acquisition fixes τ_{TJ}^{1} and only collects a subset of τ_{TJ} and τ_{TD} at a time, making it optimal for acquiring high quality data at select τ_{TJ}^{1} delays.

In asynchronous acquisition, the T-jump laser and the mid-IR probe laser are not synchronized, and the internal clock of the AFG determines when optical heating of the sample is started and stopped. Therefore, the τ_{TJ} and τ_{TD} values associated with each probe pulse are initially unknown and must be determined using an additional electronic signal. At the initiation of heating, the AFG triggers a second AFG (DG812, Rigol) to generate a 16-bit linear ramp from −10 (V_0) to 10 V (V_T) that lasts for τ_T. The voltage ramp is read by the boxcar integrator connected to the MCT array that measures the mid-IR signal. Each mid-IR shot is associated with a voltage that is related to τ_{TJ} by eq. 1.

$$V(\tau_{TJ}) = \frac{V_T - V_0}{\tau_T}\tau_{TJ} \quad (1)$$

The resolution to which τ_{TJ} and τ_{TD} values are recorded is determined by the number of voltage steps in the ramp. For a 16-bit AFG, the time resolution of the ramp is $\tau_T/2^{16}$. If τ_T is 1 s, then the time delay accuracy is limited to 15 μs.

In synchronous acquisition, the 80 MHz repetition rate from the oscillator seeding the regenerative amplifier serves as the master clock. The 80 MHz signal is divided to 1 kHz by a delay generator (SDG Elite, Coherent), which is sent to the regenerative amplifier, and the 1 kHz signal is then divided to 20 Hz. The 20 Hz signal is further divided by an integer from 2 to 256 with a programmable frequency divider (PRL-260NT, Pulse Research Lab). The resulting frequency between 0.08 Hz and 10 Hz ($1/\tau_T$) triggers the AFG to initiate a sequence of waveforms that are converted to drive the AOM and modulate the intensity the T-jump laser. The AFG sets τ_{TJ}^{1} by adding a 0 – 1 ms delay between the trigger and diffraction of T-jump laser.

For detection of nonlinear IR signals, the k_2 beam is chopped at 500 Hz, and therefore half of the mid-IR shots contain the nonlinear signal of interest and are corrected with the chopped shots to remove additional background signals. For a given T-jump event, this means that half of the τ_{TJ} and τ_{TD} delays will be chopped and the other unchopped. Ideally,

the timespan between acquisition of unchopped and chopped shots to be subtracted should be minimized to reduce the impact of fluctuations in laser power. T-jump events are acquired in pairs where the second T-jump is initiated an odd number of probe shots after initiation of the first T-jump. Therefore, every τ_{TJ} and τ_{TD} that was chopped/unchopped in the first T-jump becomes unchopped/chopped during the second T-jump, allowing for subtraction between subsequent T-jump cycles.

2.4 Temperature-Jump Linear, Pump-Probe, and 2D IR Spectroscopy

The simplest T-jump experiment, transient linear IR absorption (t-A) spectroscopy, characterizes the change in absorbance of the mid-IR spectrum observed by the probe beam as a function of τ_{TJ}. Without a separate reference detector, the t-A signal is acquired as difference between the spectral intensity at a given τ_{TJ} ($I(\omega, \tau_{TJ})$) and at the initial temperature ($I(\omega, T_i)$).

$$\Delta OD(\omega, \tau_{TJ}) = -\log\left(\frac{I(\omega, \tau_{TJ})}{I(\omega, T_i)}\right) \quad (2)$$

In practice, $I(\omega, T_i)$ is taken as the average spectral intensity at long τ_{TD} delays following re-equilibration of the sample at T_i. The measured difference spectrum then contains the time-dependent change in solvent and sample absorption. When measured on its own, the t-A signal can be acquired without optical chopping. However, when acquired simultaneously with the nonlinear IR signal, the t-A signal is extracted only from mid-IR shots where k_2 is chopped to avoid distortions from the k_2/k_3 PP and 2D IR signals.

The details of 2D IR in the pump-probe geometry have been described previously,[52–54] but a brief description of 2D IR data acquisition and processing steps will be provided. PP spectra are acquired as a function of τ_1 and Fourier transformed to give the absorptive 2D IR spectrum. The π-shifted output of the Mach-Zehnder interferometer is used to measure a pump interferogram as τ_1 is stepped. The pump interferogram is then Fourier transformed and used to correct for timing errors in τ_1 via the Mertz method.[55] All PP and 2D IR data shown here were collected with τ_2 = 100 fs. In the absence of the T-jump, PP and 2D IR data are collected as the difference in optical density (ΔOD) between adjacent mid-IR shots with k_2 unchopped (I_{open}) and chopped (I_{closed}).

$$\Delta OD(\tau_1, \tau_2, \omega_3) = -\log\left(\frac{I_{open}(\tau_1, \tau_2, \omega_3)}{I_{closed}(\tau_1, \tau_2, \omega_3)}\right) \quad (3)$$

The PP signal between k_2 and k_3 is constant during τ_1 and subtracted as the mean value over the acquired FID at each pixel.

Temperature-jump 2D IR (t-2D IR) data were acquired by stepping τ_1 and averaging for many T-jump cycles at each τ_{TJ}. Acquisitions of 90 s were performed for each τ_1 in the data shown here. To reduce acquisition time, data were undersampled along τ_1 with 24 fs steps from −160 to 2000 fs. As for equilibrium 2D IR, the mid-IR pump interferogram was used to correct for phase errors in 2D IR surfaces at each τ_{TJ} using the Mertz method.[55] t-PP and

t-2DIR spectra are typically represented as double difference spectra to emphasize spectral changes throughout the reaction.

$$\Delta\Delta OD(\omega_3, \tau_{TJ}) = -\log\left(\frac{I_{open}(\omega_3, \tau_{TJ})}{I_{closed}(\omega_3, \tau_{TJ})}\right) + \log\left(\frac{I_{open}(\omega_3, T_i)}{I_{closed}(\omega_3, T_i)}\right) \quad (4)$$

The second term in eq. 4 is the ΔOD signal at T_i prior to optical heating. The T-jump waveforms used in this study have a sufficiently long τ_{off} that allows for complete thermal relaxation of the sample prior to the next T-jump event. Therefore, spectra acquired after thermal relaxation has completed are averaged and used in the second term of eq. 4.

3. Results

3.1 Heating Profile in D_2O

3.1.1 Optimizing Heating Profile with Laser Power Waveform—CW laser-based T-jump experiments often suffer from slow rise times to a fixed T_f as well as large time-dependent deviations in T_f.[30, 56] Typically, optical heating is performed with a square power waveform where the CW laser power switches between on/off position:

$$P(t) = P_0 B(t_{on}, t_{off}) \quad (5)$$

Where the step-on/step-off function is

$$B(t_{on}, t_{off}) = 1 \quad \text{if} \; t_{on} \le t \le t_{off}$$
$$= 0 \quad \text{if} \; t < t_{on} \; \text{or} \; t > t_{off}$$

With a simple on/off power waveform, T_f is achieved once heat deposition from the T-jump laser and thermal diffusion out of the sample reach a steady-state. Our sample is placed between two CaF_2 windows spaced 50 μm apart. The thermal conductivity of CaF_2 is ~15× greater than that of D_2O, so thermal diffusion out of the sample primarily occurs through the CaF_2 windows. The blue curve in Figs. 3b and 3d show the ΔT profile (See Section S2 for determination of ΔT) for a T-jump rise with an on/off waveform and power P_0 = 1.5 W, chosen to give a steady state ΔT = 16 °C (Fig. 3a and 3c). The heating occurs in two phases: a relatively fast phase in which ~75% of the total temperature change occurs within 10 ms, and a slow phase in which heating to a steady-state continues for tens to hundreds of milliseconds. The total rise can be fit to a sum of two exponentials with time constants of 6.4 and 60 ms.

When the T-jump laser is turned off, the solvent temperature decays back to T_i, which is set by a re-circulating chiller. Traces of normalized k_3 transmission during the thermal relaxation are shown in Fig. 3d. In general, the thermal relaxation is also two phase, with most of the cooling happening quickly with a time-scale of $\tau_{D1} \approx$ 5ms, and a slower non-exponential phase. The relaxation is well fit by the sum of an exponential and stretched exponential function with minor differences between the datasets with different heating waveforms.

$$T(\tau_{TD}) = \Delta T\left[0.85\exp(-(\tau_{TD}/\tau_{D1})) + 0.15\exp\left(-(\tau_{TD}/\tau_{D2})^{\beta_D}\right)\right] + T_i \quad (6)$$

where $\tau_{D2} \approx 20$ ms and the stretch parameter (β_D) is 0.45.

To understand the heating and cooling processes and the time-dependent spatial temperature profile within the sample, the temperature distribution within the sample parallel and perpendicular to the T-jump laser beam was simulated (Fig. 4) as a function of τ_{TJ} and τ_{TD} by numerically solving the 2D heat diffusion equation in cylindrical coordinates (See Section S3 for details). After continuous heating is initiated by turning on the T-jump laser at constant intensity, the sample temperature over the mid-IR probe region exponentially increases and reaches a plateau by 10 ms (Fig. 4a), which results from the balance of energy deposited by the T-jump laser and heat flow out of the sample. Figs. 4b and 4c show the temperature distribution parallel (**r**) and perpendicular (**z**) to the CaF_2 windows during on/off heating. The temperature distribution in the **r** dimension is Gaussian with a width corresponding to the diameter of the T-jump laser spot (230 μm, $1/e^2$ in intensity), which leads to a 5% variation in ΔT across the FWHM of the mid-IR probe pulse (Fig. 4b, black line). The temperature in the z dimension (Fig. 4c) has a maximum at the center of the sample and decreases sharply near the window due to the ~15× greater thermal conductivity of CaF_2 relative to D_2O. Therefore, the temperature in the **z** dimension is the primary source of temperature inhomogeneity within the mid-IR probe volume. Once the laser is turned off, the temperature undergoes a single-exponential decay over a few milliseconds back to T_i (Fig. 4a). For both T-jump and T-drop processes, the simulations capture the relatively fast exponential first component observed in experiments but not the slow second component observed in experiment. The slow component may result from thermal relaxation within the D_2O rather than through the CaF_2 window, as suggested previously.[36] Additional simulations were performed with thermally insulating windows to enforce temperature relaxation within the D_2O (Section S4), and the resulting T-jump and T-drop profiles are similar to the slow component of the experimental profiles. However, it is still unclear why the simulations with CaF_2 windows do not reproduce the multi-exponential T-jump and T-drop behavior observed experimentally.

The thermal profile for on/off CW heating is problematic for T-jump spectroscopy as the solvent temperature rises slowly and varies substantially over most of the measured time window. We optimize the solvent heating profile with time-dependent modulation of the T-jump laser power using an AOM. To increase the rate of heating, the AOM is set to diffract the maximum amount of power for a short time (<1 ms) and then drop to a plateau power identical to the elevated power with the on/off waveform (Figs. 3a and 3c):

$$P(t) = P_{\max} B(0, 0.8\,\text{ms}) + P_0 B(0.8\,\text{ms}, 500\,\text{ms}) \quad (7)$$

The red trace in Fig. 3 illustrates a step function between two laser powers with P_{max} = 17 W and P_0 = 1.5 W, which is the simplest waveform for achieving faster heating. While the solvent temperature rises to its max value in <1 ms, it subsequently drops by nearly 20% following the step down in laser intensity and then increases back to the max temperature over tens of milliseconds. The temperature drop from 1–10 ms is also observed in T-jump

simulations (Fig. 4a) and results from an initial uneven balance between thermal diffusion out of the sample window and energy deposition due to the sudden drop in laser power. The subsequent slow rise appears similar to that observed in the on/off heating case and is not captured by the T-jump simulations.

To flatten the temperature profile at T_f, we employed more complicated power waveforms where the high-to-plateau power transition occurs via a two-component decay (green trace, Fig. 3a) rather than through a step function. This form varies the input T-jump power to more closely match the thermal diffusion out of the sample region before reaching steady-state heating:

$$P(t) = P_{\max} B\left(0, \mathrm{t_{step}}\right) + P_1 \exp\left(-\left(t - \mathrm{t_{step}}\right)/t_1\right) + P_2 \exp\left(-\left(\left(t - \mathrm{t_{step}}\right)/t_2\right)^{\beta}\right) + P_0 B\left(\mathrm{t_{step}}, 500\,\mathrm{ms}\right) \quad (8)$$

The step up (t_{step} = 0.25 ms) phase enables rapid heating but is cut short relative to the step function waveform to allow for an exponential phase (P_1=15 W, t_1=0.8 ms) that contains most of the change in power in the high-to-plateau transition. Shortening t_{step} in exchange for the exponential phase corrects for 1–10 ms temperature drop observed when the step function waveform is applied, but also extends the heating rise time from ~0.8 to ~1 ms. The remainder of the high-to-plateau power transition is a stretched-exponential decay that extends for hundreds of milliseconds (P_2 = 0.5 W, t_2 = 100 ms, β = 0.55) and corrects for the slow temperature increase observed when the step function and on/off waveforms are used. Once heated within ~1 ms, the sample maintains T_f to ± 3% (°C) over the entire T-jump time window, minimizing potential temperature-dependent artifacts in T-jump spectroscopy. Due to the time-dependent CW laser power, the solvent heating rise is not a simple exponential, as shown in Fig. 3b. The temperature profile can be fit to a compressed-exponential function.

$$T(\tau_{TJ}) = T_f - \Delta T \exp\left(-\left(\tau_{TJ}/\tau_R\right)^{\beta_R}\right) \quad (9)$$

The data in Fig. 3d was fit to a time constant (τ_R) of 0.5 ms and compression parameter (β_R) of 1.7.

3.1.2 Tunable T-Jump Magnitudes—By varying P_0, ΔT can be tuned over the temperature range of liquid D_2O (Fig. 5). Large ΔT values may amplify sample responses and expand the capability of variable T-jump measurements to study chemical kinetics for high barrier reactions.[14, 57–58] Fig. 5a shows solvent profiles for optimized T-jumps with ΔT = 4 to 75 °C. The dependence of on/off heating waveforms on ΔT is shown in Fig. S4. As ΔT increases, the rise time to T_f increases due to the reduced gap between the peak and plateau powers in the heating waveform (Fig. 5b). When fit to a compressed exponential function (Fig. 5c), τ_R increases from 0.1 to 1.8 ms while β_R drops from 1.8 to 1.4 from ΔT = 4 to 75 °C. The value of τ_R shows a linear correlation with ΔT over the range studied (Fig. 5d) and exhibits a slope of 23 μs/°C, which can be used to predict the rise time for a given ΔT. τ_{D1} also shows a subtle increase from 4.8 to 5.6 ms over the range of ΔT. To maintain a flat temperature profile at T_f, T-jump laser power waveforms need to be optimized for each ΔT (Fig. 5b). For increasing ΔT, optimization of power waveforms is accomplished by increasing t_{step} as well as increasing P_2. As a result, even for ΔT = 75 °C, the temperature

deviates only ± 2 °C (<3%) over the high temperature plateau. The parameters describing the optical waveform for each T-jump are listed in Table 1.

3.2 T-Jump IR Spectroscopy

Ubiquitin and the intercalated motif (i-motif) are studied as example systems with t-A, t-PP, and t-2D IR spectroscopy. Ubiquitin is a 76-residue protein with significant β-sheet content that has been investigated previously with optical and mixing-induced T-jump methods.[23, 57, 59] The i-motif is a class of nucleic acid structures characterized by a tetraplex mediated with cytosine-cytosine base pairs.[22, 60] The unfolding and refolding of i-motifs are known to occur slowly, as evidenced by stopped-flow measurements and hysteresis in thermal and pH melting experiments.[22, 61] However, the unfolding or refolding have yet to be studied in detail with time-resolved spectroscopy.

3.2.1 T-Jump Spectroscopy of Ubiquitin Unfolding—Fig. 6a shows the FTIR spectrum of ubiquitin from 1550 to 1740 cm^{-1} in D_2O at pH* 1. The ubiquitin spectrum overlaps with a broad D_2O bend-libration combination band that is subtracted from the raw data. The mid-IR spectrum of folded ubiquitin (Fig. 6a, low temperature) is characterized by an amide I vibration centered at 1640 cm^{-1} as well as a shoulder near 1670 cm^{-1}. The splitting of the amide I peaks arises from vibrational coupling between residues in anti-parallel β sheets.[62–63] The bright band ($\nu_\perp$) is known to have a transition dipole moment oriented perpendicular to the β-sheet while that of the shoulder ($\nu_\parallel$) is roughly parallel. Increasing the temperature toward the melting transition centered near 65 °C leads to recombination of the amide-I bands into a single broad peak centered at 1650 cm^{-1} and indicates the loss of β-sheet contacts.

The PP spectra of ubiquitin following a T-jump from 43 to 63 °C are shown in Fig. 6d. The PP spectra contain positive and negative features that arise from fundamental (0→1) and excited-state absorption (ESA) (1→2) transitions, respectively, projected onto the detection axis (ω_3). The ESA is typically shifted to lower frequency along ω_3 due to anharmonicity of the vibrational potential. The PP signal of the D_2O bend-libration combination band is negligible compared to that of the systems studied here, therefore no solvent subtraction is necessary for t-PP spectroscopy in the mid-IR. The combination of fundamental and ESA features leads to more structure in the PP spectra of ubiquitin relative to the linear absorption spectrum. In particular, a negative peak from the ESA of $\nu_\perp$ arises at 1610 cm^{-1} in addition to the two fundamental transitions. The ESA of $\nu_\parallel$ overlaps with the $\nu_\perp$ fundamental band and is not resolved in the PP spectra.

2D IR spectroscopy spreads the information content of the PP spectrum onto the excitation frequency axis (ω_1). The equilibrium 2D IR spectrum of ubiquitin at 43 °C is shown in Fig. 7a. Fundamental (red-yellow) and ESA (blue) peaks occur along and below the diagonal between the detection and excitation axis. The $\nu_\perp$ and $\nu_\parallel$ fundamental bands are each broadened along the diagonal and are not well separated in the 2D IR spectrum. The 2D IR spectrum also resolves off-diagonal features between vibrations, which may report on vibrational coupling or dynamic processes. The off-diagonal features for ubiquitin are low

amplitude for the pulse polarization scheme used here, but cross-peaks between $\nu_{\perp}$ and $\nu_{\parallel}$ have been observed with different pulse polarizations.[59]

The response of ubiquitin following a T-jump from 43 to 63 °C was probed using t-A, t-PP, and t-2D IR spectroscopy. The raw t-A difference spectra between the time-dependent linear absorption and the spectrum at T_i contain a broad background from an increase in D_2O transmission (see Fig. S5). The D_2O background is subtracted from the t-A data (Fig. 6b) using a second measurement on pure D_2O. The t-A and t-PP (Fig. 6e) difference spectra of ubiquitin are dominated by a negative feature at 1635 cm^{-1} that corresponds to the loss of the fundamental $\nu_{\perp}$ peak. Approximately 30% of the $\nu_{\perp}$ signal loss occurs within the ~1 ms heating of the sample. The remaining signal change occurs over tens of milliseconds and can be described by a single-exponential decay with a time constant of 30 ms. t-2D IR difference spectra are presented at τ_{TJ} values of 3 and 100 ms in Fig. 7b and time traces at select probe frequencies are shown in Fig. 7c. Red changes indicate a gain or loss of a positive or negative 2D IR feature, respectively, while blue changes correspond to negative gain or positive loss. The 3 ms surface exhibits negative and positive change in the $\nu_{\perp}$ fundamental and ESA transitions, respectively, with additional positive change above the diagonal. There is also a negative/positive doublet observed at the $\nu_{\parallel}$ transition. By 100 ms, the $\nu_{\perp}$ difference features are approximately 3× greater and a negative/positive doublet is clearly observed at the lower-right cross-peak region between $\nu_{\perp}$ and $\nu_{\parallel}$, indicating the loss of β-sheet content. T-jump time-traces at select 2D IR features are plotted in Fig. 7c and reveal relaxation kinetics identical to those observed in the t-A and t-PP data.

The T-jump response for ubiquitin reveals fast (<1 ms) and slow (10–100 ms) phases of unfolding characterized by the loss β-sheet content (Figs. 6c and 7b), which is consistent with previous pulsed T-jump IR studies.[57, 59, 64] The fast phase was previously characterized as downhill unfolding occurring from 100 ns to 100 μs that results from rapidly shifting a subensemble of folded molecules at T_i to the unfolding transition state at T_f. The remaining unfolding transitions must surpass a large free energy barrier and correspond to the slow unfolding phase. Pulsed T-jump 2D IR could directly observe the fast unfolding phase, but the time window of these previous experiments was limited by thermal relaxation of the sample on the order of milliseconds, and the complete activated unfolding process could not be measured. In this work, we can measure the entire activated unfolding process that occurs from 10 to 100 ms. Overall, ubiquitin illustrates one example where multiple T-jump methods are needed to resolve the entire unfolding dynamics of a protein.

Once the T-jump laser is turned off, the solvent thermally equilibrates back to T_i while ubiquitin re-folds. As discussed above, the solvent cooling is significantly slower than the heating timescales, and the re-folding response may be distorted by the time-dependent temperature of the sample. At the studied temperature, the T-drop relaxation response of ubiquitin lags behind the solvent cooling and the majority of signal change occurs between 10 and 100 ms (Fig. 6f). However, the T-drop relaxation profile is more complicated than a single exponential and is better described by the sum of two stretched exponentials where the latter likely arises from the slow thermal relaxation component of the solvent.

3.2.2 T-Jump Spectroscopy of i-Motif Unfolding—

5’-CCCTTTCCCTTTCCCTTTCCC-3’ (C3T3) is chosen as a model sequence to investigate slow nucleic acid folding due to its known preference to adopt a unimolecular i-motif structure.[65] Fig. 8a shows an FTIR temperature series of C3T3 at pH* 4.5 from 3 to 97 °C. The random coil single-strand dominates at the highest temperature and exhibits many in-plane nucleobase vibrations from 1550 to 1750 cm^{-1}.[38, 66–67] The peak at 1701 cm^{-1} and shoulder at 1720 cm^{-1} correspond to thymine and protonated cytosine carbonyl stretch vibrations, respectively. The brightest peak at 1656 cm^{-1} is dominated by cytosine carbonyl stretch vibrations and overlaps with a mixed carbonyl/ring thymine stretch. The shoulder at 1632 cm^{-1} corresponds to a thymine ring vibration while the peak and shoulder at 1613 and 1577 cm^{-1} each correspond to cytosine ring modes. Upon i-motif formation, the most noticeable spectral change is the splitting of the 1656 cm^{-1} band into peaks centered at 1665 and 1700 cm^{-1} Additionally, the shoulder at 1720 cm^{-1} and band at 1577 cm^{-1} are suppressed while the 1613 cm^{-1} shoulder redshifts to 1609 cm^{-1}. The PP spectrum of C3T3 is similar to the FTIR spectrum in that it contains three positive peaks at 1632, 1665, and 1700 cm^{-1} at low temperature (Fig. 8d). The spectral region from 1550 to 1620 cm^{-1} has negative amplitude and is structured due to overlap of multiple ESA features. The 2D IR spectrum of C3T3 (Fig. 9a) fully resolves each of the fundamental/ESA doublets between 1550 and 1740 cm^{-1}. Off-diagonal features are observed between the 1632 and 1665 cm^{-1} peaks as well as between the 1665 and 1700 cm^{-1} peaks and indicate coupling between nucleobase vibrations.[39, 41]

The response of C3T3 following a T-jump from 45 to 65 °C was probed using t-A (Fig. 8b), t-PP (Fig. 8e), and t-2D IR spectroscopy (Fig. 9b). Regardless of the IR probe, the relaxation response of C3T3 spans many tens of milliseconds (Fig. 8c). The D_2O background was subtracted from t-A spectra using a second measurement on pure D_2O. However, a second method for background removal using a discrete wavelet transform (DWT) approach is also demonstrated for C3T3 (Fig. S5). As τ_{TJ} increases from 0.1 to 500 ms, the t-A spectra exhibit a primary gain feature at 1656 cm^{-1} as well as a gain and loss at 1720 and 1700 cm^{-1}, respectively. Each of difference features are consistent with the spectral changes in the FTIR temperature series, suggesting that the relaxation response corresponds to unfolding of C3T3. The t-PP spectra also have a primary gain feature at 1656 cm^{-1}, but it is narrower than that in the t-A spectra due to overlap with ESA bands at higher and lower frequency. A net loss in amplitude is observed from 1550 to 1620 cm^{-1} due to a gain in magnitude of the brightest ESA peak, and additional peaks result from the fundamental and ESA transitions of cytosine ring vibrations.

Due to the many fundamental and ESA transitions exhibited by C3T3 between 1550 and 1740 cm^{-1}, the changes in the t-PP spectra (Fig. 8e) are more difficult to interpret than for ubiquitin (Fig. 6). The t-2D IR spectra in Fig. 9b clarify many of the assignments in the t-PP spectra as well as provide additional spectral information that may be useful for describing detailed structural dynamics. At 5 ms, the t-2D IR spectrum of C3T3 reveals a modest gain from 1640 – 1670 cm^{-1} along ω_1 at ω_3 = 1650 cm^{-1} with a negative growth at (ω_1,ω_3) = (1650 cm^{-1}, 1630 cm^{-1}). By 100 ms, these difference features have substantially increased in amplitude and indicate a redshift of the fundamental and ESA at ω_1 = 1665 cm^{-1} to ω_1 =

1650 cm^{-1}. Additionally, positive loss is observed near (1700 cm^{-1}, 1700 cm^{-1}) and (1730 cm^{-1}, 1700 cm^{-1}) whereas positive gain appears at (1700 cm^{-1}, 1675 cm^{-1}) and (1720 cm^{-1}, 1720 cm^{-1}). The loss and redshift of the 1700 cm^{-1} and 1665 cm^{-1} diagonal features, respectively, are consistent with recombination of the C_2=O carbonyl vibrational modes split upon i-motif formation. The growth along the diagonal at 1720 cm^{-1} indicates a gain of protonated cytosine in the random coil state. In agreement with the t-A and t-PP data, the t-2D IR features capture i-motif unfolding from 1 to 100 ms, but also allow for a more detailed analysis of transient changes in coupling, line shape, and spectral shifts.

Figs. 8c and 9c show T-jump relaxation kinetics for C3T3 probed at the main difference feature at 1656 cm^{-1}. The t-A, t-PP, and t-2D IR data exhibit a single component unfolding response that is well-fit to a stretched exponential function with a time constant of ~25 ms and stretch parameter of 0.85. Stretched exponential kinetics are commonly observed in biomolecular reactions and result from a distribution of reaction rates that may report on structural heterogeneity or multiple reaction pathways.[12, 58, 68] In T-jump experiments, temperature heterogeneity throughout the probe volume of the sample may also lead to a distribution of reaction rates for activated processes and artificially stretched relaxation kinetics. From the C3T3 data alone, it is impossible to distinguish whether the stretched exponential kinetics arise from a temperature artifact or molecular properties of the system. However, similar stretched exponential behavior would be expected from ubiquitin if caused by a temperature artifact, but ubiquitin exhibits single-exponential unfolding kinetics consistent with previous reports.[23, 57, 64] Assuming the unfolding barrier for C3T3 is not significantly larger than that of ubiquitin, then the stretched exponential kinetics of C3T3 indicate a heterogeneity of starting states or unfolding pathways rather than an artifact from temperature inhomogeneity.

Similar to ubiquitin, the T-drop relaxation of C3T3 lags behind the solvent thermal relaxation by many milliseconds. However, the observed time trace is still best described by the sum of an exponential and a long-lived stretched exponential. The first exponential has a time constant of ~24 ms while the second is ~100 ms with a stretch parameter of 0.55. The presence of the second slow component suggests that the re-folding response is distorted by the solvent cooling profile. As T_f increases (Fig. S9), the re-folding timescale increases, and the time profile becomes a single stretched exponential, which further suggests that the slow component at T_f = 45 °C results from distortion by the solvent profile. A detailed discussion and analysis of distortions in the T-jump and T-drop profiles are provided in Section S7.

4. Discussion & Conclusions

The instrument presented here extends the accessible time window of T-jump 2D IR spectroscopy by five orders of magnitude, allowing the enhanced information content of 2D IR to be applied to the study of structural dynamics and kinetics from 1 ms to many seconds. As shown for the model i-motif in this work, many molecules that unfold or dissociate over many milliseconds also fold or associate on slow enough timescales to be separated from the solvent thermal relaxation. Therefore, in many cases T-jump and T-drop measurements will be able to simultaneously probe each direction of a reaction, which typically requires a combination of mixing and T-jump experiments.[15, 69]

In previous transient 2D IR experiments, detection of the probe signal occurs with a repetition rate much lower than the reaction timescale of interest and t-2D IR acquisition must be repeated at many trigger delays to fully sample the process. Therefore, t-2D IR has typically been used for coarse probing of reactions in time whereas 1D probes are employed for fine sampling of kinetics.[19, 51, 70–72] However, there are many experiments in which evolution of a cross-peak or lineshape over the course of a reaction provides quantitative dynamic information and requires fine sampling with t-2D IR.[73] Even though the repetition rate of the mid-IR probe is the same as those used in previous t-2D IR methods, the relaxation timescales of interest are much slower and can therefore be monitored finely in time with t-2D IR spectroscopy. The time traces shown in Figs. 7c and 9c demonstrate the ability of our instrument to probe reactions finely in time with t-2D IR.

The high-power CW T-jump laser enables ΔT to be adjusted across the temperature range of liquid D_2O and modulation of the laser power with the AOM provides tunability to the T-jump waveform, both of which will extend our capability to probe the dynamics and physical properties of a reaction. For example, experiments where T_f is fixed and T_i is varied have been used to probe the shape of unfolding and dissociation barriers as well as folded and dimer state wells, but such measurements have been limited to ΔT of 20 °C in pulsed optical T-jumps.[14, 57–58] The larger ΔT tunability from our t-2D IR spectrometer will enable greater reshaping of the free energy surface for both fixed T_f and fixed T_i measurements. The measurements in this work utilized a simple T-jump waveform in which the temperature was repeatedly jumped to T_f and relaxed to T_i. However, more complicated T-jump waveforms could be utilized to probe nonequilibrium dynamics. For example, following an initial T-jump, a second T-jump may be used to perturb the system at different time points along its evolution to the first T_f. This scheme is one of many imaginable waveforms that could be easily implemented with an intensity modulated T-jump source.

One aspect of the t-2D IR spectrometer in this work that can be improved is the solvent heating rise time. T-jump kinetic simulations (See Section S7) predict that the observed rate will become distorted toward slower values as the reaction rate increases. As ΔT increases, the solvent heating time also increases with a slope of 23 μs/°C, which, depending on the timescales of interest, may further distort the observed signal. Thermally insulating films may be useful for reducing the rise time for a given ΔT by extending the lifetime of heat exchange out of the sample. The rise time may also be shortened by reducing the spot size of the T-jump laser, which will increase the input energy density at the sample but may also lead to thermal artifacts due to temperature heterogeneity in dimensions parallel to the window.

Lastly, we note that the T-jump setup described in this study will be used in complement with a previously reported t-2D IR spectrometer that uses pulsed optical heating to probe T-jump responses from 10 ns to 1 ms.[7] Nucleic acids and proteins often exhibit a hierarchy of structural dynamics ranging from changes in solvation on picosecond timescales to large changes in secondary structure over hundreds of microseconds to seconds. In combination, our setups can monitor T-jump responses from 10 ns to seconds with the same experimental probe, allowing for a broadly spanning characterization of the motions exhibited by a biomolecule across many decades in time.

Supplementary Material

Refer to Web version on PubMed Central for supplementary material.

Acknowledgements

This work was supported by the National Institute of General Medical Sciences of the National Institutes of Health (Award No. R01GM118774). B.A. acknowledges support from the NSF Graduate Research Fellowship Program. We thank Kathryn Segner for assistance in data acquisition and careful reading of the manuscript.

References

1. Gruebele M; Sabelko J; Ballew R; Ervin J, Laser temperature jump induced protein refolding. Acc. Chem. Res 1998, 31, 699–707.
2. Callender R; Dyer RB, Probing protein dynamics using temperature jump relaxation spectroscopy. Curr. Opin. Struc. Biol 2002, 12, 628–633.
3. Pörschke D; Eigen M, Co-operative non-enzymatic base recognition III. Kinetics of the helix—coil transition of the oligoribouridylic oligoriboadenylic acid system and of oligoriboadenylic acid alone at acidic pH. J. Mol. Biol 1971, 62, 361–381. [PubMed: 5138337]
4. Williams AP; Longfellow CE; Freier SM; Kierzek R; Turner DH, Laser temperature-jump, spectroscopic, and thermodynamic study of salt effects on duplex formation by dGCATGC. Biochemistry 1989, 28, 4283–4291. [PubMed: 2765487]
5. Kubelka J, Time-resolved methods in biophysics. 9. Laser temperature-jump methods for investigating biomolecular dynamics. Photochem. Photobiol. Sci 2009, 8, 499–512. [PubMed: 19337664]
6. Hoffman GW, A nanosecond temperature-jump apparatus. Rev. Sci. Instrum 1971, 42, 1643–1647.
7. Chung HS; Khalil M; Smith AW; Tokmakoff A, Transient two-dimensional IR spectrometer for probing nanosecond temperature-jump kinetics. Rev. Sci. Instrum 2007, 78, 063101. [PubMed: 17614599]
8. Thompson MC; Barad BA; Wolff AM; Cho HS; Schotte F; Schwarz DM; Anfinrud P; Fraser JS, Temperature-jump solution X-ray scattering reveals distinct motions in a dynamic enzyme. Nat. Chem 2019, 11, 1058–1066. [PubMed: 31527847]
9. Ballew R; Sabelko J; Reiner C; Gruebele M, A single-sweep, nanosecond time resolution laser temperature-jump apparatus. Rev. Sci. Instrum 1996, 67, 3694–3699.
10. Williams S; Causgrove TP; Gilmanshin R; Fang KS; Callender RH; Woodruff WH; Dyer RB, Fast events in protein folding: helix melting and formation in a small peptide. Biochemistry 1996, 35, 691–697. [PubMed: 8547249]
11. Turner DH; Flynn GW; Sutin N; Beitz JV, Laser Raman temperature-jump study of the kinetics of the triiodide equilibrium. Relaxation times in the 10^{-8}-10^{-7} second range. J. Am. Chem. Soc 1972, 94, 1554–1559.
12. Sabelko J; Ervin J; Gruebele M, Observation of strange kinetics in protein folding. Proc. Natl. Acad. Sci 1999, 96, 6031–6036. [PubMed: 10339536]
13. Yang WY; Gruebele M, Folding at the speed limit. Nature 2003, 423, 193–197. [PubMed: 12736690]
14. Sanstead PJ; Tokmakoff A, Direct observation of activated kinetics and downhill dynamics in DNA dehybridization. J. Phys. Chem. B 2018, 122, 3088–3100. [PubMed: 29504399]
15. Narayanan R; Zhu L; Velmurugu Y; Roca J; Kuznetsov SV; Prehna G; Lapidus LJ; Ansari A, Exploring the energy landscape of nucleic acid hairpins using laser temperature-jump and microfluidic mixing. J. Am. Chem. Soc 2012, 134, 18952–18963. [PubMed: 23078026]
16. Ansari A; Kuznetsov SV; Shen Y, Configurational diffusion down a folding funnel describes the dynamics of DNA hairpins. Proc. Natl. Acad. Sci 2001, 98, 7771–7776. [PubMed: 11438730]
17. Ruasse MF; Aubard J; Galland B; Adenier A, Kinetic study of the fast halogen-trihalide ion equilibria in protic media by the Raman-laser temperature-jump technique. A non-diffusion-controlled ion-molecule reaction. J. Phys. Chem 1986, 90, 4382–4388.

18. Kao J; TsIEN RY, Ca2+ binding kinetics of fura-2 and azo-1 from temperature-jump relaxation measurements. Biophys. J 1988, 53, 635–639. [PubMed: 3382715]
19. Peng CS; Baiz CR; Tokmakoff A, Direct observation of ground-state lactam–lactim tautomerization using temperature-jump transient 2D IR spectroscopy. Proc. Natl. Acad. Sci 2013, 110, 9243–9248. [PubMed: 23690588]
20. Kubota J; Yoda E; Ishizawa N; Wada A; Domen K; Kano SS, Site-Hopping of Adsorbed CO in c (4× 2)-CO/Ni (111) by Laser-Induced Temperature Jump: Time-Resolved Sum-Frequency Generation Observation. J. Phys. Chem. B 2003, 107, 10329–10332.
21. Gray RD; Chaires JB, Kinetics and mechanism of K+-and Na+-induced folding of models of human telomeric DNA into G-quadruplex structures. Nucleic Acids Res 2008, 36, 4191–4203. [PubMed: 18567908]
22. Abou Assi H; Garavís M; González C; Damha MJ, i-Motif DNA: structural features and significance to cell biology. Nucleic Acids Res. 2018, 46, 8038–8056. [PubMed: 30124962]
23. Noronha M; Gerbelová H; Faria TQ; Lund DN; Smith DA; Santos H; Maçanita AL, Thermal unfolding kinetics of ubiquitin in the microsecond-to-second time range probed by Tyr-59 fluorescence. J. Phys. Chem. B 2010, 114, 9912–9919. [PubMed: 20666531]
24. Marchand A; Czar MF; Eggel EN; Kaeslin J; Zenobi R, Studying biomolecular folding and binding using temperature-jump mass spectrometry. Nat. Commun 2020, 11, 1–12. [PubMed: 31911652]
25. Torrent J; Marchal S; Ribó M; Vilanova M; Georges C; Dupont Y; Lange R, Distinct unfolding and refolding pathways of ribonuclease a revealed by heating and cooling temperature jumps. Biophys. J 2008, 94, 4056–4065. [PubMed: 18234832]
26. Phillips RS; Miles EW; McPhie P; Marchal S; Georges C; Dupont Y; Lange R, Pressure and temperature jump relaxation kinetics of the conformational change in Salmonella typhimurium tryptophan synthase L-serine complex: large activation compressibility and heat capacity changes demonstrate the contribution of solvation. J. Am. Chem. Soc 2008, 130, 13580–13588. [PubMed: 18795779]
27. Sicard F; Destainville N; Manghi M, DNA denaturation bubbles: Free-energy landscape and nucleation/closure rates. J. Chem. Phys 2015, 142, 034903. [PubMed: 25612729]
28. Holmstrom ED; Dupuis NF; Nesbitt DJ, Pulsed IR heating studies of single-molecule DNA duplex dissociation kinetics and thermodynamics. Biophys. J 2014, 106, 220–231. [PubMed: 24411254]
29. Holmstrom ED; Nesbitt DJ, Real-time infrared overtone laser control of temperature in picoliter H2O samples: “nanobathtubs” for single molecule microscopy. J. Phys. Chem. Lett 2010, 1, 2264–2268. [PubMed: 21814589]
30. Polinkovsky ME; Gambin Y; Banerjee PR; Erickstad MJ; Groisman A; Deniz AA, Ultrafast cooling reveals microsecond-scale biomolecular dynamics. Nat. Commun 2014, 5, 5737. [PubMed: 25517430]
31. Fritzsch R; Greetham GM; Clark IP; Minnes L; Towrie M; Parker AW; Hunt NT, Monitoring base-specific dynamics during melting of DNA–ligand complexes using temperature-jump time-resolved infrared spectroscopy. J. Phys. Chem. B 2019, 123, 6188–6199. [PubMed: 31268327]
32. Brewer SH; Vu DM; Tang Y; Li Y; Franzen S; Raleigh DP; Dyer RB, Effect of modulating unfolded state structure on the folding kinetics of the villin headpiece subdomain. Proc. Natl. Acad. Sci 2005, 102, 16662–16667. [PubMed: 16269546]
33. Hauser K; Krejtschi C; Huang R; Wu L; Keiderling TA, Site-specific relaxation kinetics of a tryptophan zipper hairpin peptide using temperature-jump IR spectroscopy and isotopic labeling. J. Am. Chem. Soc 2008, 130, 2984–2992. [PubMed: 18278908]
34. Dyer RB; Gai F; Woodruff WH; Gilmanshin R; Callender RH, Infrared studies of fast events in protein folding. Acc. Chem. Res 1998, 31, 709–716.
35. Panman MR; van Dijk CN; Meuzelaar H; Woutersen S, Nanosecond folding dynamics of an alpha helix: Time-dependent 2D-IR cross peaks observed using polarization-sensitive dispersed pump-probe spectroscopy. J. Chem. Phys 2015, 142, 041103. [PubMed: 25637962]
36. Ma H; Ervin J; Gruebele M, Single-sweep detection of relaxation kinetics by submicrosecond midinfrared spectroscopy. Rev. Sci. Instrum 2004, 75, 486–491.

37. Stancik AL; Brauns EB, Rearrangement of partially ordered stacked conformations contributes to the rugged energy landscape of a small RNA hairpin. Biochemistry 2008, 47, 10834–10840. [PubMed: 18808148]
38. Banyay M; Sarkar M; Gräslund A, A library of IR bands of nucleic acids in solution. Biophys. Chem 2003, 104, 477–488. [PubMed: 12878315]
39. Peng CS; Jones KC; Tokmakoff A, Anharmonic vibrational modes of nucleic acid bases revealed by 2D IR spectroscopy. J. Am. Chem. Soc 2011, 133, 15650–15660. [PubMed: 21861514]
40. Sanstead PJ; Stevenson P; Tokmakoff A, Sequence-dependent mechanism of DNA oligonucleotide dehybridization resolved through infrared spectroscopy. J. Am. Chem. Soc 2016, 138, 11792–11801. [PubMed: 27519555]
41. Krummel AT; Zanni MT, DNA vibrational coupling revealed with two-dimensional infrared spectroscopy: Insight into why vibrational spectroscopy is sensitive to DNA structure. J. Phys. Chem. B 2006, 110, 13991–14000. [PubMed: 16836352]
42. Lee C; Cho M, Vibrational dynamics of DNA. II. Deuterium exchange effects and simulated IR absorption spectra. J. Chem. Phys 2006, 125, 114509. [PubMed: 16999492]
43. Ganim Z; Chung HS; Smith AW; DeFlores LP; Jones KC; Tokmakoff A, Amide I two-dimensional infrared spectroscopy of proteins. Acc. Chem. Res 2008, 41, 432–441. [PubMed: 18288813]
44. Kim YS; Hochstrasser RM, Applications of 2D IR spectroscopy to peptides, proteins, and hydrogen-bond dynamics. J. Phys. Chem. B 2009, 113, 8231–8251. [PubMed: 19351162]
45. Jones KC; Peng CS; Tokmakoff A, Folding of a heterogeneous β-hairpin peptide from temperature-jump 2D IR spectroscopy. Proc. Natl. Acad. Sci 2013, 110, 2828–2833. [PubMed: 23382249]
46. Brewer SH; Song B; Raleigh DP; Dyer RB, Residue specific resolution of protein folding dynamics using isotope-edited infrared temperature jump spectroscopy. Biochemistry 2007, 46, 3279–3285. [PubMed: 17305369]
47. Scheerer D; Chi H; McElheny D; Keiderling TA; Hauser K, Enhanced Sensitivity to Local Dynamics in Peptides by Use of Temperature-Jump IR Spectroscopy and Isotope Labeling. Chem. Eur. J 2019, 26, 3524–3534.
48. Huang C-Y; Getahun Z; Wang T; DeGrado WF; Gai F, Time-Resolved Infrared Study of the Helix − Coil Transition Using 13C-Labeled Helical Peptides. J. Am. Chem. Soc 2001, 123, 12111–12112. [PubMed: 11724630]
49. Khalil M; Demirdöven N; Tokmakoff A, Coherent 2D IR spectroscopy: Molecular structure and dynamics in solution. J. Phys. Chem. A 2003, 107, 5258–5279.
50. Roberts ST; Loparo JJ; Tokmakoff A, Characterization of spectral diffusion from two-dimensional line shapes. J. Chem. Phys 2006, 125, 084502. [PubMed: 16965024]
51. Sanstead PJ; Ashwood B; Dai Q; He C; Tokmakoff A, Oxidized Derivatives of 5-Methylcytosine Alter the Stability and Dehybridization Dynamics of Duplex DNA. J. Phys. Chem. B 2020, 124, 1160–1174.
52. DeFlores LP; Nicodemus RA; Tokmakoff A, Two-dimensional Fourier transform spectroscopy in the pump-probe geometry. Optics letters 2007, 32, 2966–2968. [PubMed: 17938668]
53. Hamm P; Zanni M, Concepts and methods of 2D infrared spectroscopy. Cambridge University Press: Cambridge, UK 2011.
54. Helbing J; Hamm P, Compact implementation of Fourier transform two-dimensional IR spectroscopy without phase ambiguity. J. Opt. Soc. Am. B 2011, 28, 171–178.
55. Mertz L, Auxiliary computation for Fourier spectrometry. Infrared Phys. 1967, 7, 17–23.
56. Steinhoff HJ, A continuous wave laser T-jump apparatus and its application to chemical reactions in hemoglobin single crystals. J. Biochem. Bioph. Meth 1988, 15, 319–330.
57. Chung HS; Tokmakoff A, Temperature-dependent downhill unfolding of ubiquitin. I. Nanosecond-to-millisecond resolved nonlinear infrared spectroscopy. Proteins. 2008, 72, 474–487. [PubMed: 18384151]
58. Leeson DT; Gai F; Rodriguez HM; Gregoret LM; Dyer RB, Protein folding and unfolding on a complex energy landscape. Proc. Natl. Acad. Sci 2000, 97, 2527–2532. [PubMed: 10681466]

59. Chung HS; Ganim Z; Jones KC; Tokmakoff A, Transient 2D IR spectroscopy of ubiquitin unfolding dynamics. Proc. Natl. Acad. Sci 2007, 104, 14237–14242. [PubMed: 17551015]
60. Gehring K; Leroy J-L; Guéron M, A tetrameric DNA structure with protonated cytosine-cytosine base pairs. Nature 1993, 363, 561–565. [PubMed: 8389423]
61. Chen C; Li M; Xing Y; Li Y; Joedecke C-C; Jin J; Yang Z; Liu D, Study of pH-induced folding and unfolding kinetics of the DNA i-motif by stopped-flow circular dichroism. Langmuir 2012, 28, 17743–17748. [PubMed: 23148777]
62. Krimm S; Bandekar J, Vibrational spectroscopy and conformation of peptides, polypeptides, and proteins In Advances in protein chemistry, Elsevier: Cambridge, MA 1986; Vol. 38, pp 181–364. [PubMed: 3541539]
63. Byler DM; Susi H, Examination of the secondary structure of proteins by deconvolved FTIR spectra. Biopolymers 1986, 25, 469–487. [PubMed: 3697478]
64. Chung HS; Khalil M; Smith AW; Ganim Z; Tokmakoff A, Conformational changes during the nanosecond-to-millisecond unfolding of ubiquitin. Proc. Natl. Acad. Sci 2005, 102, 612–617. [PubMed: 15630083]
65. Školáková P; Renčiuk D; Palacký J; Krafčík D; Dvořáková Z; Kejnovská I; Bednářová K; Vorlíčková M, Systematic investigation of sequence requirements for DNA i-motif formation. Nucleic Acids Res. 2019, 47, 2177–2189. [PubMed: 30715498]
66. Petrovic AG; Polavarapu PL, Structural transitions in polyribocytidylic acid induced by changes in pH and temperature: vibrational circular dichroism study in solution and film states. J. Phys. Chem. B 2006, 110, 22826–22833. [PubMed: 17092034]
67. Tsankov D; Krasteva M; Andrushchenko V; van de Sande J; Wieser H, Vibrational circular dichroism signature of hemiprotonated intercalated four-stranded i-DNA. Biophys. Chem 2006, 119, 1–6. [PubMed: 16183193]
68. Johnston D, Stretched exponential relaxation arising from a continuous sum of exponential decays. Phys. Rev. B 2006, 74, 184430.
69. Chen C; Wang W; Wang Z; Wei F; Zhao XS, Influence of secondary structure on kinetics and reaction mechanism of DNA hybridization. Nucleic Acids Res. 2007, 35, 2875–2884. [PubMed: 17430963]
70. Bredenbeck J; Helbing J; Behrendt R; Renner C; Moroder L; Wachtveitl J; Hamm P, Transient 2D-IR spectroscopy: Snapshots of the nonequilibrium ensemble during the picosecond conformational transition of a small peptide. J. Phys. Chem. B 2003, 107, 8654–8660.
71. Xiong W; Laaser JE; Paoprasert P; Franking RA; Hamers RJ; Gopalan P; Zanni MT, Transient 2D IR spectroscopy of charge injection in dye-sensitized nanocrystalline thin films. J. Am. Chem. Soc 2009, 131, 18040–18041. [PubMed: 19947603]
72. Kolano C; Helbing J; Kozinski M; Sander W; Hamm P, Watching hydrogen-bond dynamics in a β-turn by transient two-dimensional infrared spectroscopy. Nature 2006, 444, 469–472. [PubMed: 17122853]
73. Tucker MJ; Abdo M; Courter JR; Chen J; Brown SP; Smith AB; Hochstrasser RM, Nonequilibrium dynamics of helix reorganization observed by transient 2D IR spectroscopy. Proc. Natl. Acad. Sci 2013, 110, 17314–17319. [PubMed: 24106309]

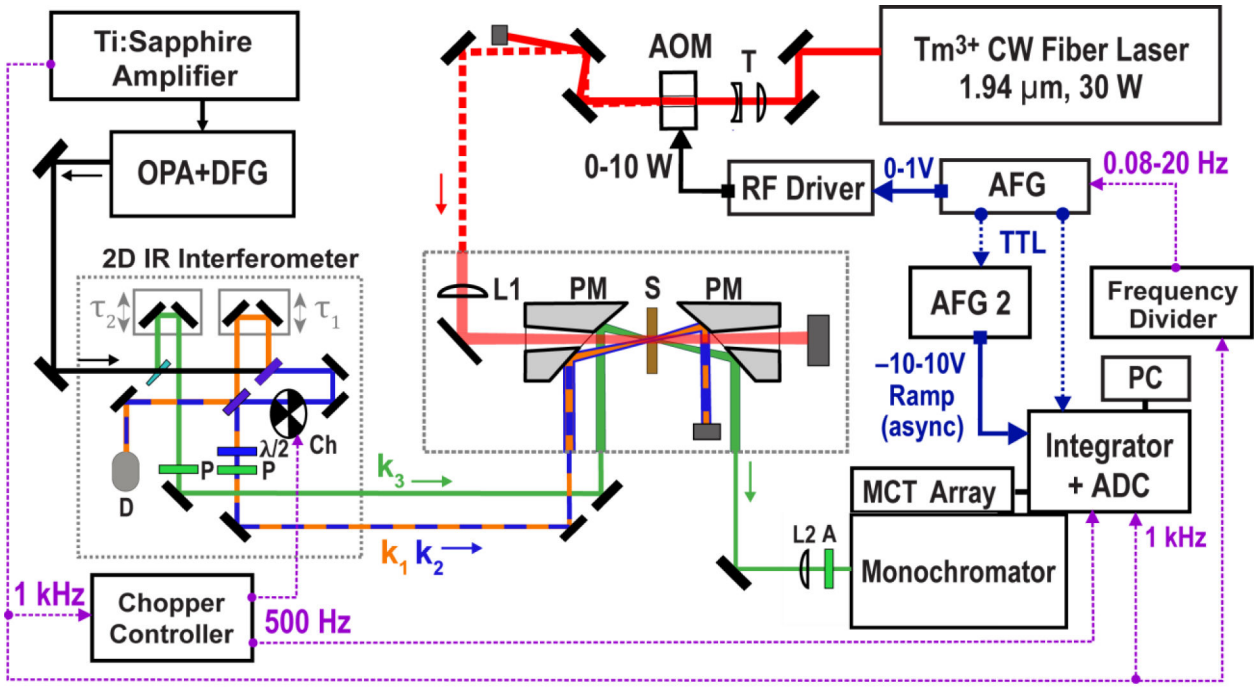

Figure 1.

Diagram of optical setup and relevant electronic components for t-2D IR, t-PP, and t-A data acquisition. D – room temperature MCT detector, Ch – optical chopper, λ/2 – half waveplate, P – polarizer, L1 – T-jump focusing lens (f = 30 cm), PM – parabolic mirror (RFL = 2 in), S – sample, T – telescope, AOM – TeO_2 acousto-optic modulator, AFG – arbitrary function generator, PC – host computer, L2 – focusing lens into monochromator (f = 10 cm), A - analyzer.

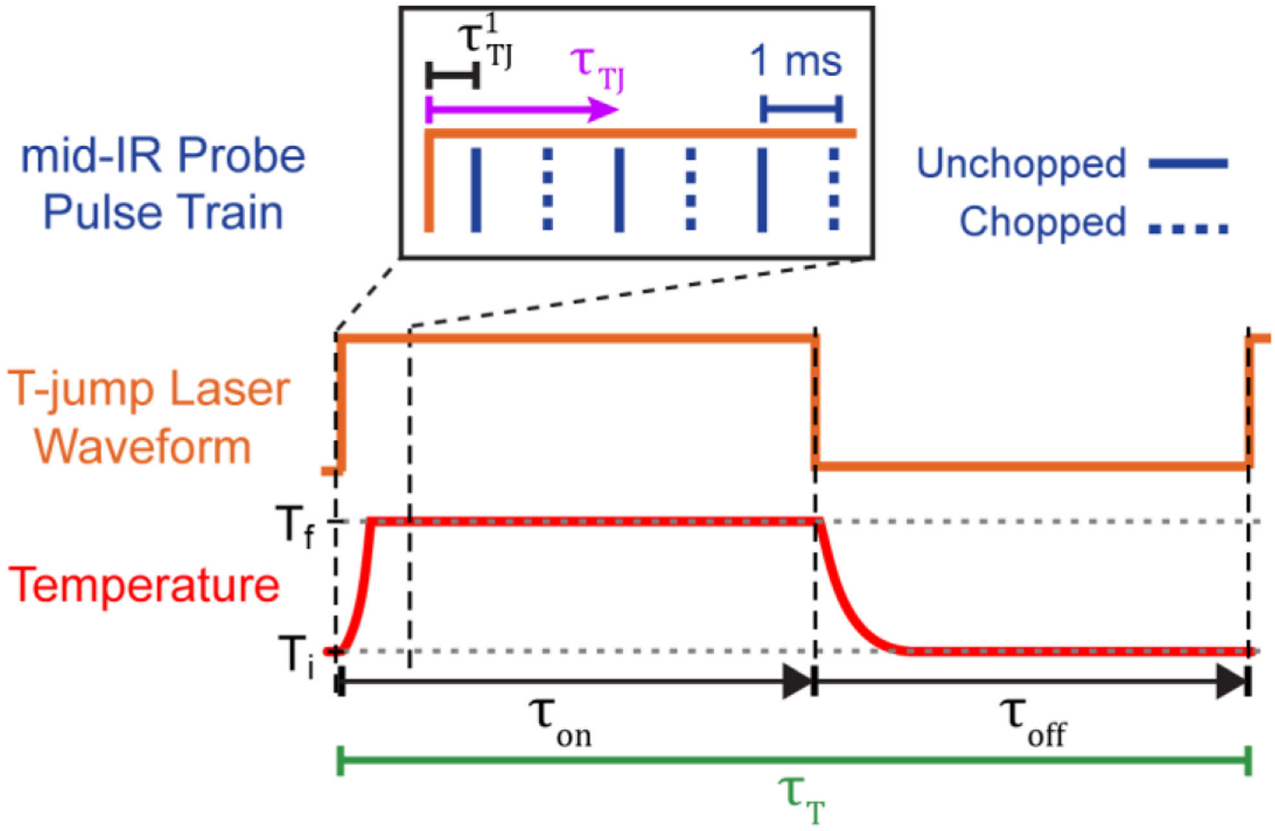

Figure 2.

Schematic of timing between optical heating and arrival of mid-IR probe. The first mid-IR probe shot arrives between 0 and 1 ms (τ_{TJ}^{1}) after optical heating is initiated, and subsequent probe shots arrive every 1 ms. τ_{TJ}^{1} can be electronically controlled or allowed to wander due to the mismatch in mid-IR probe and T-jump ($1/\tau_T$) repetition rate. T_f is held for hundreds of milliseconds to seconds (τ_{on}) while probe shots are collected according to their time of arrival after heating is initiated (τ_{TJ}). At τ_{on}, the laser is switched off for another period of hundreds of milliseconds to seconds (τ_{off}), and probe shots are tracked as a function of time after the T-jump laser turns off. For detection of nonlinear IR probe signals, every other mid-IR shot is chopped (dashed line). T-jump events are collected in pairs where the second T-jump cycle is delayed 1 ms relative to the first, allowing for chopper subtraction between adjacent T-jump events.

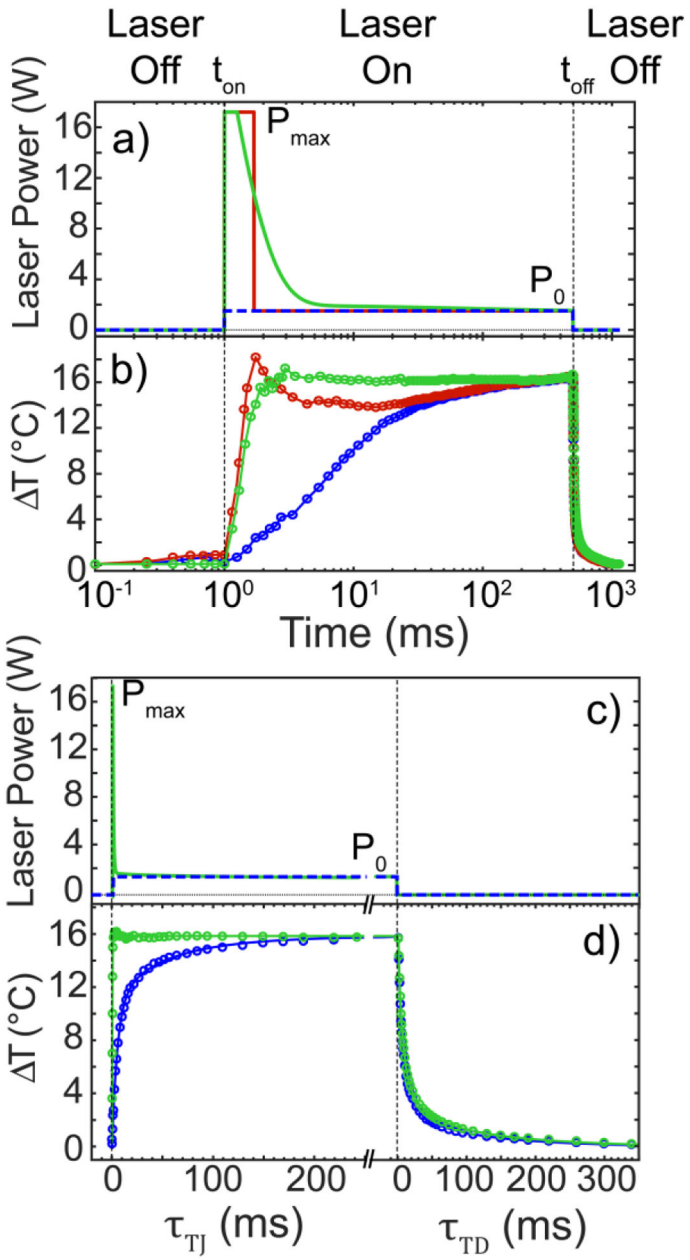

Figure 3.

(a) Semi-log plot of T-jump laser power at the sample as a function of time for different amplitude modulation waveforms applied to the AOM, and (b) the corresponding change in solvent temperature (ΔT) as a function of time for different T-jump laser power waveforms. Measurements were performed at T_i = 20 °C. ΔT was computed using the method described in Section S2. (c,d) Similar figures to (a) and (b) on a linear time axis. The on/off (blue) and optimized (green) rise profiles are fit to bi-exponential ($\tau(1)$ = 6.4 ms, $\tau(2)$ = 60 ms) and compressed (τ_R = 0.5 ms, β_R = 1.7) exponential functions, respectively. Solvent cooling profiles are fit to bi-exponential decays (τ_{D1} = 5.1 ms, τ_{D2} = 20 ms).

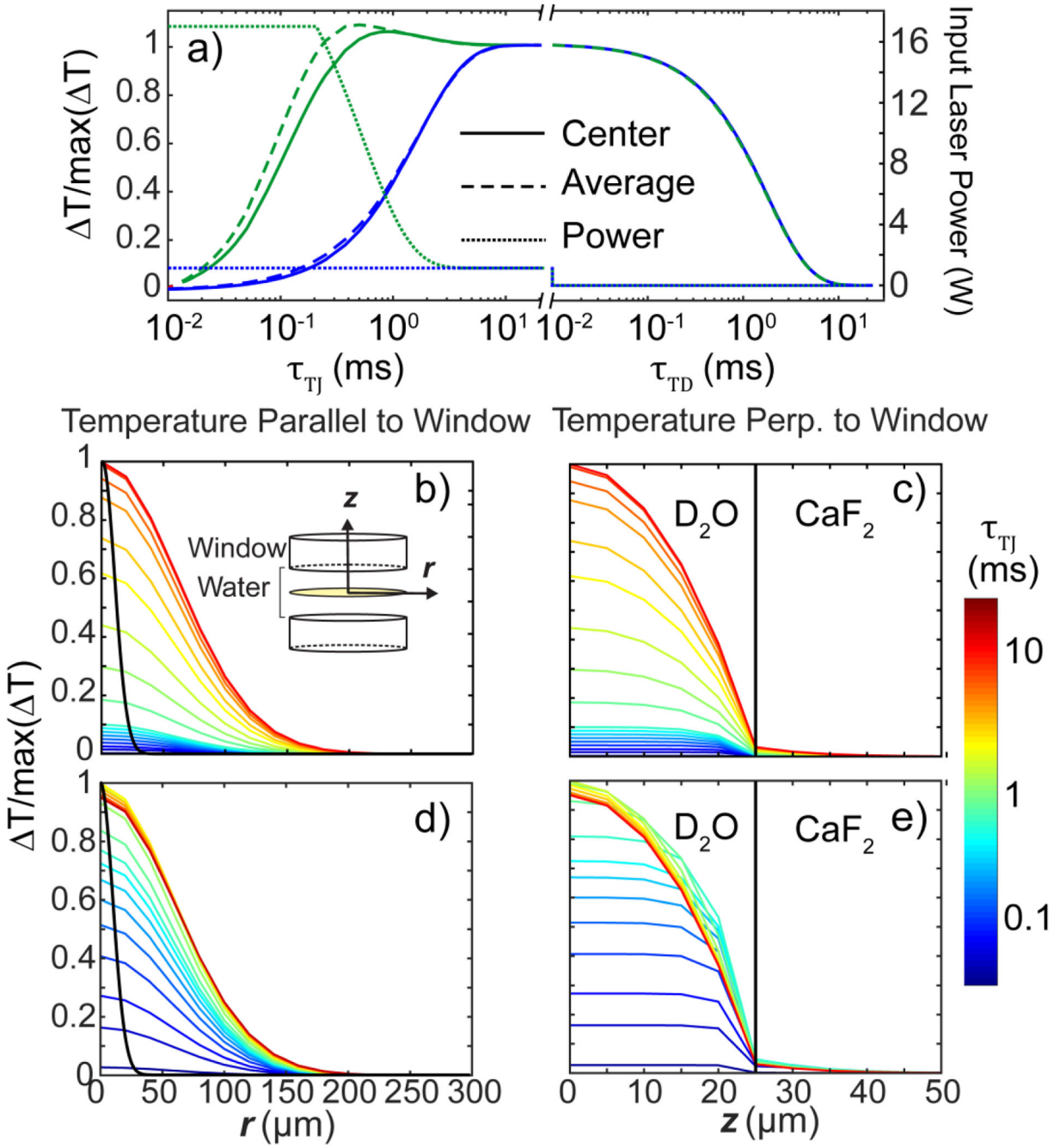

Figure 4.

Numerical simulations of ΔT during T-jump laser heating and cooling. (a) Normalized ΔT at center of T-jump laser focus (solid) and averaged across the heated region perpendicular (**z**) to the sample window and mid-IR probe area parallel (**r**) to the window (dash). Temperature profiles for on/off (blue line) and high-to-plateau power (green line) are shown. Input laser power as a function of τ_{TJ} and τ_{TD} are plotted for each waveform (dotted line). (b) Normalized ΔT distribution radially along the beam axis for on/off T-jump in 20 μm steps. The Gaussian profile of the mid-IR probe at the sample focus is overlaid in black. Inset shows the cylindrical coordinate system for the simulation. (c) Normalized ΔT distribution

perpendicular to the sample window for on/off T-jump in 5 μm steps. (d,e) Similar plots for high-to-plateau power T-jumps.

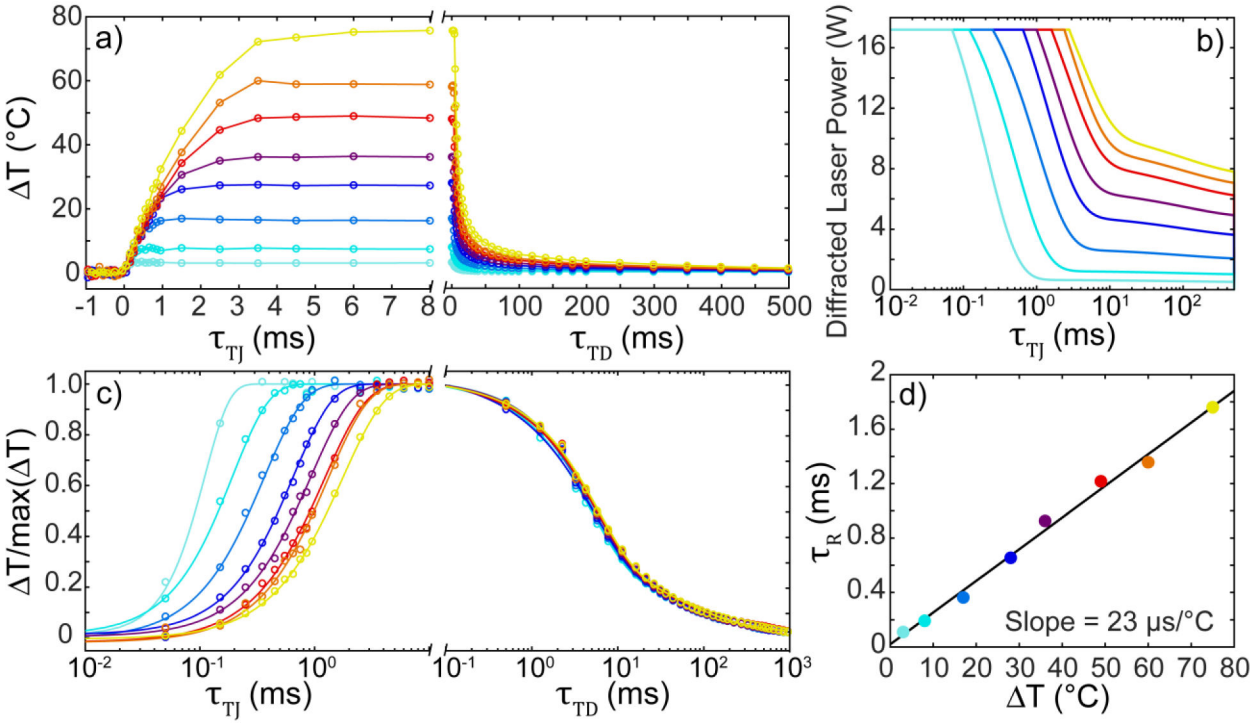

Figure 5.

(a) ΔT determined from mid-IR probe transmission as a function of τ_{TJ} and τ_{TD} for maximum ΔT ranging from 4 to 75 °C. Measurements were performed at T_i = 5 °C. (b) T-jump laser power at the sample as a function of time for various ΔT. (c) Normalized mid-IR probe transmission curves upon heating and cooling. Heating traces are fit to eq. 9 (solid line) with time constant τ_R and compression parameter β_R while cooling traces are fit to eq. 6 with time constants τ_{D1}, τ_{D2}, and stretch parameter β_D. (d) τ_R as a function of ΔT (dots) fit to a linear function (solid). The fit gives a slope of 23 μs per °C.

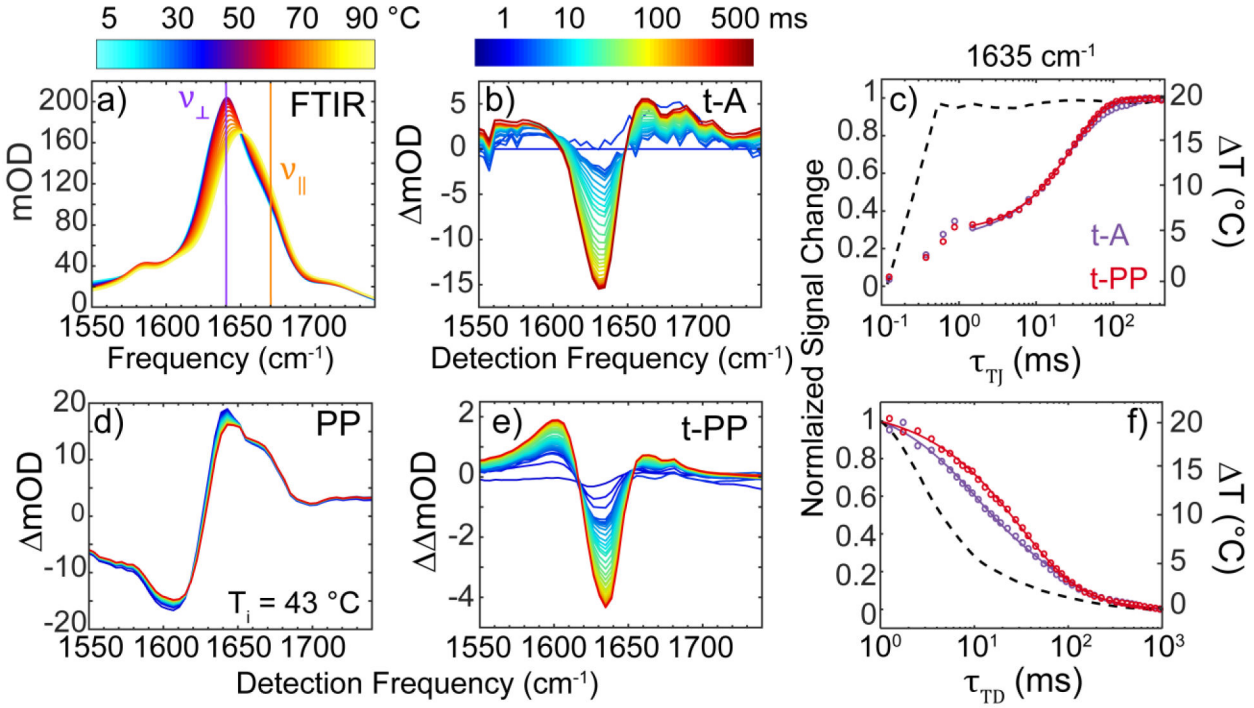

Figure 6.

(a) Equilibrium FTIR temperature series of ubiquitin from 3 to 97 °C. (b) t-A difference, (d) pump-probe (PP), and (e) pump-probe difference (t-PP) spectra from τ_{TJ} = 0.1 to 500 ms following a T-jump from 43 to 63 °C. (c) T-jump and (f) T-drop t-A and t-PP time traces probed at 1635 cm^{-1}. Dashed lines indicate solvent heating and cooling traces. T-jump time traces are fit (solid lines) to a single-exponential rise at τ_{TJ} > 1 ms. T-drop time traces are fit to a sum of two stretched exponentials.

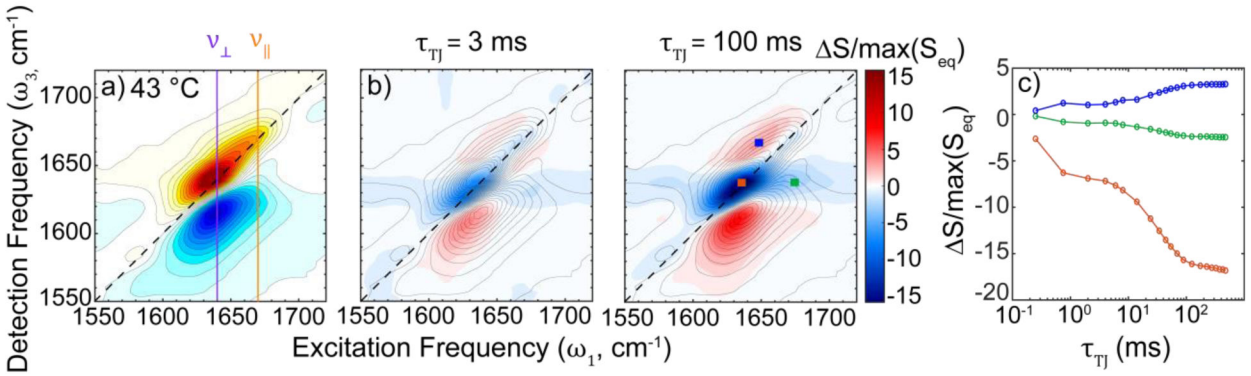

Figure 7.

(a) 2D IR spectrum of ubiquitin at 43 °C acquired with a parallel (ZZZZ) polarization scheme and τ_2 = 100 fs. (b) T-jump 2D IR (t-2D IR) difference spectra acquired at τ_{TJ} = 3 and 100 ms following a T-jump from 43 to 63 °C. The contour map of the equilibrium surface is superimposed on the difference spectra. Red indicates a positive gain or negative loss while blue corresponds to negative gain or positive loss. Difference amplitudes are plotted in percent change relative to the maximum of the equilibrium spectrum. (c) Time traces probed at select features on the t-2D IR surfaces marked by the colored squares in (b).

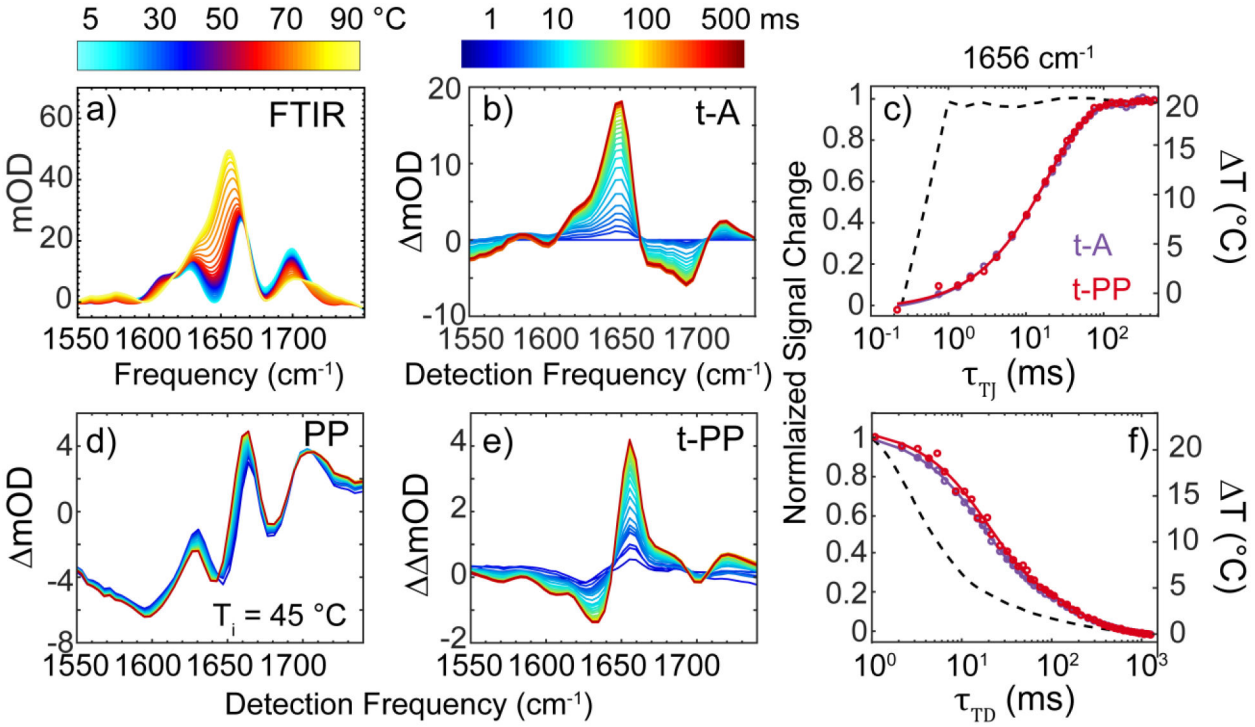

Figure 8.

(a) Equilibrium FTIR temperature series of C3T3 from 3 to 97 °C. (b) t-A difference, (d) PP, and (e) t-PP spectra from τ_{TJ} = 0.1 to 500 ms following a T-jump from 45 to 65 °C. (c) T-jump and (f) T-drop t-A (purple) and t-PP (red) time traces probed at 1656 cm^{-1}. Dashed lines indicate solvent heating and cooling traces. T-jump traces are fit to a single stretched exponential (solid lines) while T-drop traces are fit to a sum of two stretched exponentials.

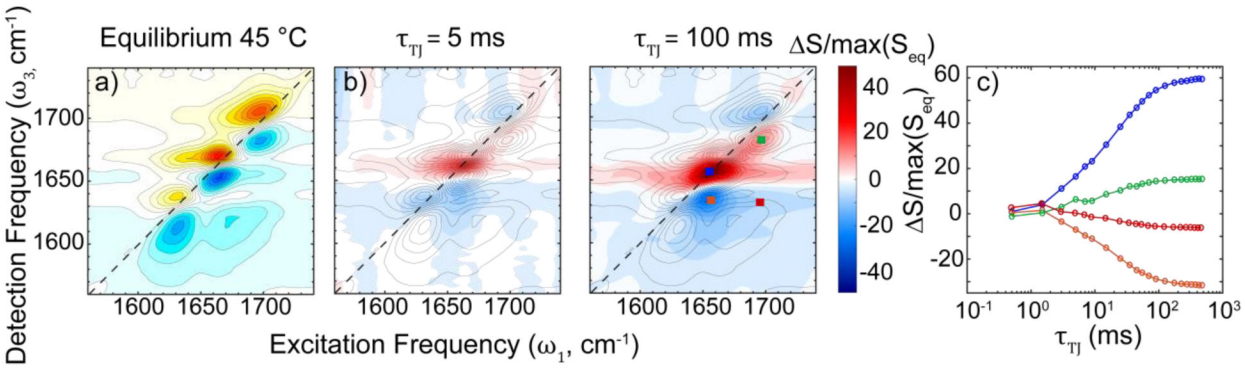

Figure 9.

(a) 2D IR spectrum of C3T3 at 45 °C acquired with a parallel (ZZZZ) polarization scheme and τ_2 = 100 fs. (b) t-2D IR difference spectra acquired at τ_{TJ} = 4 and 100 ms following a T-jump from 45 to 65 °C. The contour map of the equilibrium surface is superimposed on the difference spectra. Red indicates a positive gain or negative loss while blue corresponds to negative gain or positive loss. Difference amplitudes are plotted in percent change relative to the maximum of the equilibrium spectrum. (c) Time traces probed at select features on the t-2D IR surfaces marked by the colored squares in (b).

Table 1.

Optical waveform parameters for variable ΔT shown in Fig. 5

AT (°C)	4	9	18	29	38	50	60	75
P_{max} (W)	17.3	17.3	17.3	17.3	17.3	17.3	17.3	17.3
t_{step} (ms)	0.07	0.12	0.25	0.65	1.0	1.6	2.4	2.8
P_1 (W)	16.7	16.1	14.6	12.3	10.8	8.7	7.6	6.5
t_1 (ms)	0.2	0.5	1.0	1.4	1.9	2.7	3.1	4.0
P_2 (W)	0.15	0.25	0.75	1.5	2.0	2.6	2.9	3.3
t_2 (ms)	100	100	100	100	100	100	100	100
β	0.55	0.55	0.55	0.55	0.55	0.55	0.55	0.55
P_0 (W)	0.5	1.0	2.0	3.5	4.5	6.0	6.8	7.5